Geophysical Research Letters

RESEARCH LETTER

10.1029/2018GL077902

Key Points:
- Magnetotail current sheet properties at lunar distances are revealed
- Magnetic field shear makes a significant contribution to the pressure balance for 50% of observed current sheets
- Intense field-aligned currents 1–10 nA/m^2) exist at the lunar distance magnetotail

Correspondence to:
A. Runov,
arunov@igpp.ucla.edu

Citation:
Xu, S., Runov, A., Artemyev, A., Angelopoulos, V., & Lu, Q. (2018). Intense cross-tail field-aligned currents in the plasma sheet at lunar distances. *Geophysical Research Letters*, *45*, 4610–4617. https://doi.org/10.1029/2018GL077902

Received 12 MAR 2018
Accepted 23 APR 2018
Accepted article online 9 MAY 2018
Published online 22 MAY 2018

Intense Cross-Tail Field-Aligned Currents in the Plasma Sheet at Lunar Distances

Sixue Xu[1,2], Andrei Runov[1], Anton Artemyev[1,3], Vassilis Angelopoulos[1], and Quanming Lu[2]

[1]Department of Earth, Planetary, and Space Sciences and Institute of Geophysics and Planetary Physics, University of California, Los Angeles, CA, USA, [2]CAS Key Laboratory of Geospace Environment, Department of Geophysics and Planetary Sciences, University of Science and Technology of China, Hefei, China, [3]Space Research Institute, RAS, Moscow, Russia

Abstract Field-aligned currents in the Earth's magnetotail, typically observed at the plasma sheet boundary layer, are believed to be driven by transient plasma flows and strong plasma pressure gradients at equatorial footpoints. Magnetotail currents (transverse to the magnetic field), usually observed within the plasma sheet, flow duskward (cross-tail) and are believed to be diamagnetic. These two current systems, field aligned and transverse, can be easily distinguished because of their differing propagation direction. By statistically analyzing magnetotail current sheet crossings by the two lunar-orbiting Acceleration, Reconnection, Turbulence and Electrodynamics of Moon's Interaction with the Sun spacecraft (probes), we demonstrate that the duskward magnetotail current in the lunar distance magnetotail ($\sim$ 55–65 R_E) can, at times, be predominantly field aligned. In about half the current sheet crossings examined, there is a significant equatorial, unidirectional cross-tail magnetic field component near the peak cross-tail current density. Because of the alignment of the magnetic field with the cross-tail current, a significant part of the total cross-tail current ($\sim$1 to 10 nA/m^2) is field aligned. This magnetic field component contributes significantly to the vertical pressure balance and is therefore important for plasma sheet dynamic stability. The generation mechanism and closure of the resultant field-aligned current system and its role in the dynamic stability of the current sheet are important to investigate further.

Plain Language Summary The continuous solar wind stream deforms the dipole magnetic field of the Earth forming the region of the stretched field, known as the magnetotail. It extends into the space far beyond Moon's orbit, which is 60 R_E away from the Earth. The magnetotail confines a hot plasma layer, the plasma sheet. The main magnetic field component changes its direction at the magnetic equator. It was established that this change in the field direction occurs in a thin layer called the magnetotail current sheet. The current sheet is the key region in the magnetosphere, because an instability in it results in an explosive release of the magnetic energy. These processes cause magnetic storms. In this work, we studied the structure of the magnetotail current sheet at lunar distances by probing it with two lunar-orbiting satellites, Acceleration, Reconnection, Turbulence and Electrodynamics of Moon's Interaction with the Sun (ARTEMIS) 1 and 2. We found that the structure of the current sheet at lunar distances significantly differs from that in the near-Earth magnetotail. This is the important information that allows us to better understand the magnetotail current sheet stability.

1. Introduction

Current sheets are essential elements in the dynamics of large-scale plasma systems, such as planetary magnetotails (e.g., Eastwood et al., 2015, and references therein). Earth's magnetotail current sheet, which is readily accessible to observations by spacecraft, is a high-β region in which the plasma pressure significantly exceeds the magnetic field pressure. Models describing such a magnetic configuration predict a diamagnetic cross-tail current flowing from dawn to dusk, transverse to the magnetic field (see, e.g., Birn et al., 2004; Sitnov & Merkin, 2016; Zelenyi et al., 2011, and references therein). In the near-Earth plasma sheet, the geometry of which is determined by the Earth's dipole magnetic field, strong deviations from the nominal geometry and the formation of cross-tail currents flowing locally along magnetic field lines have been observed only rarely during dynamic events, such as reconnection (Nakamura et al., 2008) and high-amplitude plasma sheet flapping (e.g., Petrukovich et al., 2015, and references therein).

At lunar distances, however, the magnetotail is influenced by solar wind conditions rather than by Earth's dipole field (see, e.g., Sibeck & Lin, 2014, and references therein), and the average north-south component, B_z (geocentric solar magnetospheric [GSM] coordinates are used throughout this paper), is smaller than its fluctuations. Additionally, transient intense currents (e.g., Hoshino et al., 1996; Pulkkinen et al., 1993; Vasko et al., 2015) make the magnetotail current sheet very dynamical and unstable. Therefore, one can expect more complicated current sheet configurations in the tail at lunar distances than in the near-Earth tail.

We investigate magnetotail current sheet properties at lunar distances ($\sim$60 R_E) using observations from the two Acceleration, Reconnection, Turbulence and Electrodynamics of Moon's Interaction with the Sun (ARTEMIS) probes. We select current sheet crossings during plasma sheet flapping in order to use the measured plasma velocity normal to the current sheet to convert time variations to spatial scales and thus infer current densities (Sergeev et al., 1998). Statistical studies of these current sheet observations reveal a previously unknown property of this magnetotail region: in about half the 130 events examined, the current sheet contains a strong dawn-to-dusk magnetic field component, peaking at the current sheet center (at the location of peak current density). Because this component is a sizeable fraction of the lobe field, it contributes significantly to pressure balance. In these events, therefore, the cross-tail current, also typically in the dawn-to-dusk direction, is largely field aligned. (The magnitude of this current varies from $\sim$1 to 10 nA/m^2, comparable to or larger than typical cross-tail currents at lunar distances.) Similar, largely field-aligned currents have been observed in the solar wind (e.g., Paschmann et al., 2013) and in planetary magnetotails, where the plasma pressure is so small that it is insufficient to maintain the pressure balance (e.g., Jupiter, Venus, and Mars; see Artemyev et al., 2014, 2017; Rong et al., 2015).

2. Data Set and Analysis Technique

Since July 2011 both ARTEMIS probes (P1 and P2) have been in stable, equatorial, high-eccentricity, 26-hr orbits ($\sim$100 km $\times$ 19,000 km altitude) around the Moon. The probe separation varies between 500 km and 5 R_E. The ARTEMIS pair traverses the magnetotail for about 4 days per month. We use ARTEMIS fluxgate magnetometer measurements (four vectors per second in fast survey; see Auster et al., 2008) and ion moments from combined electrostatic analyzer (ESA; energies below $\sim$ 25 keV; McFadden et al., 2008) and solid state telescope (Angelopoulos et al., 2008) instrument data. For electron moments, we use only ESA measurements (no Solid State Detector (SST) measurements above 35 keV are necessary because electron temperatures are typically no more than a few keV). To achieve the necessary time resolution, we use only data obtained during the fast survey mode of operations, predominantly on the magnetotail's duskside ($Y_{GSM} > 0$), which provides 3-D distributions of ions and electrons at spin period cadence (the maximum possible).

From 1 year of ARTEMIS observations (June 2016 to June 2017), we visually select rapid, complete current sheet crossings (130 events), each identified as a B_x reversal within less than 20 min having a B_x span larger than 5 nT. To determine the local coordinate system, we use minimum variance analysis, an orthogonalization technique of the 3-D matrix of variances in the fields during the crossing, which results in $\boldsymbol{l}$, $\boldsymbol{m}$, and $\boldsymbol{n}$ eigenvectors of maximum, intermediate, and minimum variances, respectively (Sonnerup & Cahill Jr. 1968). The maximum variance direction is mainly along the sign-changing component (B_x); the minimum variance direction is interpreted as the normal to the plane of the current sheet (i.e., the direction of the main gradient); and the intermediate variance direction is therefore along the (typically cross-tail) current direction.

For all current sheet crossings, we confirmed that pressure balance $B_l^2 + B_m^2 + 2k_B\mu_0 n_e(T_i + T_e) = B_{\rm lobe}^2 \approx$ const was satisfied to within 20% (n_e, T_i, and T_e are electron density and ion and electron temperatures, respectively, and pressure isotropy is assumed). We investigate two distinct categories of current sheets with different pressure balances: (1) current sheets with $B_{\rm lobe}^2 \gg B_m^2$, where the lobe pressure is fully balanced by the thermal plasma pressure $2k_B\mu_0 n_e(T_e + T_i)$, and (2) current sheets with B_m^2 comparable to $B_{\rm lobe}^2$, where the lobe pressure is partially balanced by the magnetic pressure from the B_m component. In the latter category, we find that B_m^2 most often peaks around the equatorial plane $B_l = 0$, and its variation across the **current** sheet ΔB_m^2 is comparable to $\Delta B_l^2 \approx B_{\rm lobe}^2$. Figure 1a shows the spatial distribution of current sheets with $\Delta B_m^2/B_{\rm lobe}^2 < 0.2$ and $\Delta B_m^2/B_{\rm lobe}^2 > 0.2$ (with $B_m \gtrapprox 0.4B_{\rm lobe}$). A significant number of the selected current sheets are characterized by a B_m contribution to the pressure balance. This is a distinct feature of the lunar distance magnetotail; in the near-Earth tail, current sheets with $B_m \gtrapprox 0.4B_{\rm lobe}$ are observed only rarely (see examples in Nakamura et al., 2008; Rong et al., 2012).

10.1029/2018GL077902

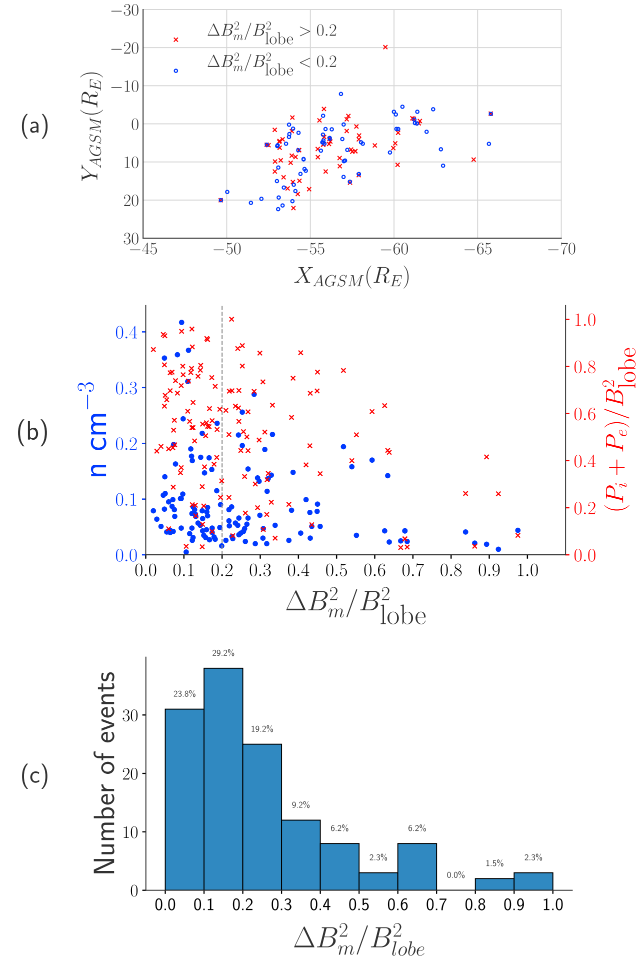

Figure 1. (a) Distribution of current sheets with $\Delta B_m^2/B_{\mathrm{lobe}}^2 < 0.2$ (blue circles) and $\Delta B_m^2/B_{\mathrm{lobe}}^2 > 0.2$ (red crosses). (b) Plasma density and thermal pressure in the current sheet center $|B_l| < 0.4B_{\mathrm{lobe}}$ nT as functions of $\Delta B_m^2/B_{\mathrm{lobe}}$. (c) Histogram of $\Delta B_m^2/B_{\mathrm{lobe}}^2$.

Figure 1b illustrates the correlation between plasma density, normalized thermal pressure ($2k_B\mu_0 n_e(p_i + p_e)/B_{\mathrm{lobe}}^2$), and $\Delta B_m^2/B_{\mathrm{lobe}}^2$. The points are concentrated mainly on the lower left side; that is, events with large $\Delta B_m^2/B_{\mathrm{lobe}}^2$ are characterized by low density (low plasma pressure), whereas those with small $\Delta B_m^2/B_{\mathrm{lobe}}^2$ are characterized by high density (thermal pressure). As shown in Figure 1c, 53% of the 130 events fall into the first category ($\Delta B_m^2/B_{\mathrm{lobe}}^2 < 0.2$), and 47% (the remainder) are broadly distributed, with $\Delta B_m^2/B_{\mathrm{lobe}}^2$ ranging from 0.2 to 1.0.

3. Current Sheet Structure

To investigate the structure of the current sheets with large $\Delta B_m^2/B_{\mathrm{lobe}}^2$, we select six events with a v_z (or $\boldsymbol{v}\cdot\boldsymbol{n}$) velocity that correlates well with $\mathrm{d}B_l/\mathrm{d}t$; this selection enables us to use the vertical profile reconstruction technique (Sergeev et al., 1998). Table 1 shows the minimum variance analysis results, the average interplanetary magnetic field (IMF) B_y during 30 min prior to current sheet crossings, and the main current sheet parameters for the selected events (A–E).

The current density **j** and the current sheet spatial scale (L) for each crossing were estimated using linear regression between $\mathrm{d}B_l/\mathrm{d}t$ and v_z: $j_m \sim (\mathrm{d}B_l/\mathrm{d}t)/v_z$, $j_l \sim (\mathrm{d}B_m/\mathrm{d}t)/v_z$. Table 1 shows that j_m reaches 10 nA/m^2, which is a very large value even when compared with the near-Earth current density values (see Petrukovich et al., 2015, for review). Current sheet thicknesses are about 500–1,000 km, comparable to an ion gyroradius in a lobe magnetic field, which indicates that the observed current sheets are thin. The magnitude of the j_l current is comparable with that of j_m, which indicates that the electric current geometry in the selected events

Table 1
Characteristic Parameters of Selected Crossings

Case	Probe	Date	Time	Duration (s) (s)	λ_m/λ_n	$\Delta B_m^2/B_{\text{lobe}}^2$	IMF B_y (nT)	Fit to	$\angle n_z/n_y$ (deg)	B_{lobe} (nT)	N_e (cm^{-3})	p_e+p_i (nT^2)	j_l (nA/m^2)	j_m (nA/m^2)	L (km)	L/ρ_i
A	B	2017-04-13	01:02:38	430	2.149	0.253	−1.27	v_n	2.7	7.30	0.20	47.36	0.45	1.25	4895	11.05
B	B	2017-01-11	18:37:00	40	15.000	0.552	−0.97	v_z	47.2	8.78	0.04	39.28	−9.06	−12.16	492	0.76
C	B	2017-01-11	11:40:33	193	7.042	0.593	−0.45	v_z	31.2	8.76	0.17	46.70	2.50	−2.05	1721	3.90
D	B	2016-11-13	19:48:18	147	16.601	0.317	0.76	v_z	40.8	11.85	0.02	24.06	8.06	−13.53	516	1.17
E	C	2016-10-15	08:08:06	317	6.322	0.634	−6.68	v_z	31.5	14.46	0.14	92.75	−11.09	8.90	689	1.91
F	C	2017-01-11	10:45:16	985	1.864	0.02	0.60	v_z	46.5	9.66	0.08	81.37	0.00	−0.69	5404	8.07

Note. Dates are formatted as year/month/day.

is different from the typical cross-tail current geometry, in which $j_l \sim 0$. For comparison, we also selected one example of a strongly tilted (vertical) current sheet with well-correlated v_n and $\mathrm{d}B_l/\mathrm{d}t$ but without significant ΔB_m^2 (event F from Table 1).

The top six panels of Figure 2 show time series of magnetic field components in the $\{l, m, n\}$ coordinate system and the calculated lobe field strength, B_{lobe}. It is apparent that $B_{\text{lobe}} \approx$ const. In events A–E, a B_m peak around the equatorial plane $B_l = 0$ is evident. A significant n_y component indicates that the current sheets are tilted in the YZ plane (Zhang et al., 2002), so both B_y and B_z (GSM) contribute to the B_m component, and the current flows partially in the north-south direction. The middle six panels of Figure 2 show profiles of plasma and magnetic (due to ΔB_m^2) pressures versus B_l. In the five events (A–E), the B_m contribution to the pressure balance is comparable to the thermal plasma contribution. The plasma pressure variation across the current sheets is supported by both density and temperature variations (see bottom six panels of Figure 2). The apparent temperature increase in event C at the current sheet boundary is caused by rarefied, hot, field-aligned ion flows that do not contribute to the pressure balance. Strong density variations across the sheet in events A, E, and F are notable. In contrast, in the near-Earth magnetotail the density variation is usually much weaker than the temperature variation $T_i(B_l)$ across the sheet (e.g., Petrukovich et al., 2015; Runov et al., 2006).

To reconstruct the current sheet structure, we adopt methods used by Sergeev et al. (1998) and Vasko et al. (2015). First, we determine the time interval during which there is a good correlation between the derivative $\mathrm{d}B_l/\mathrm{d}t$ of the 16-s smoothed magnetic field and the v_n (or v_z) velocity. Then we integrate the velocity (excluding offset v_0 defined from $v_z = (\mathrm{d}B_l/\mathrm{d}t)/(\mu_0 j_m) + v_0$ through data fitting) during this interval to determine the z coordinate (note that in the figures we use $z^* = z - z_0$ where z_0 is defined from $z^* = 0$ at $B_l = 0$). We fit $B_l(z)$ and $B_m(z)$ dependencies with the simple functions $\tan h(z/L)$, $\cos h^{-1}(z/L)$, respectively (see model in Harrison & Neukirch, 2009). The reconstructed magnetic field profiles are shown in the top six panels of Figure 3. In events A to E the B_m component exhibits a bell-shaped profile, $B_m \sim \cos h^{-1}(z/L)$, with the current sheet thickness L about a few ion gyroradii.

The bottom six panels in Figure 3 show current density profiles computed using the fitted magnetic field components. In events A to E, the current sheet has a strong $j_m \sim$1–10 nA/m^2 peak and bipolar j_l profiles. Because of this large B_m, almost all measured cross-tail current is field aligned. The transverse current magnitude is several times smaller than the field-aligned current magnitude. Because the m direction differs from event to event, the measured field-aligned current can be positive or negative without any correspondence to the IMF direction. In event F, the current profile is characterized by rather weak $j_m \sim$0.5 nA/m^2, which is a typical current density magnitude at such distances (Vasko et al., 2015).

4. Discussion and Conclusions

The observations of unexpectedly strong field-aligned currents at lunar distances open important issues regarding magnetotail current sheet stability. First, magnetic reconnection in the distant magnetotail current sheet (at lunar distances and beyond) plays an important role in the configuration of the entire magnetotail and plasma dynamics. Reconnection properties in current sheets with strong field-aligned currents are significantly different from those in Harris-type current sheets (see, e.g., Fan et al., 2016; Wilson et al., 2016; Zhou et al., 2015). Therefore, more detailed investigations (both simulations and spacecraft data analysis) of magnetic reconnection in current sheets at lunar distances are required. Second, the

10.1029/2018GL077902

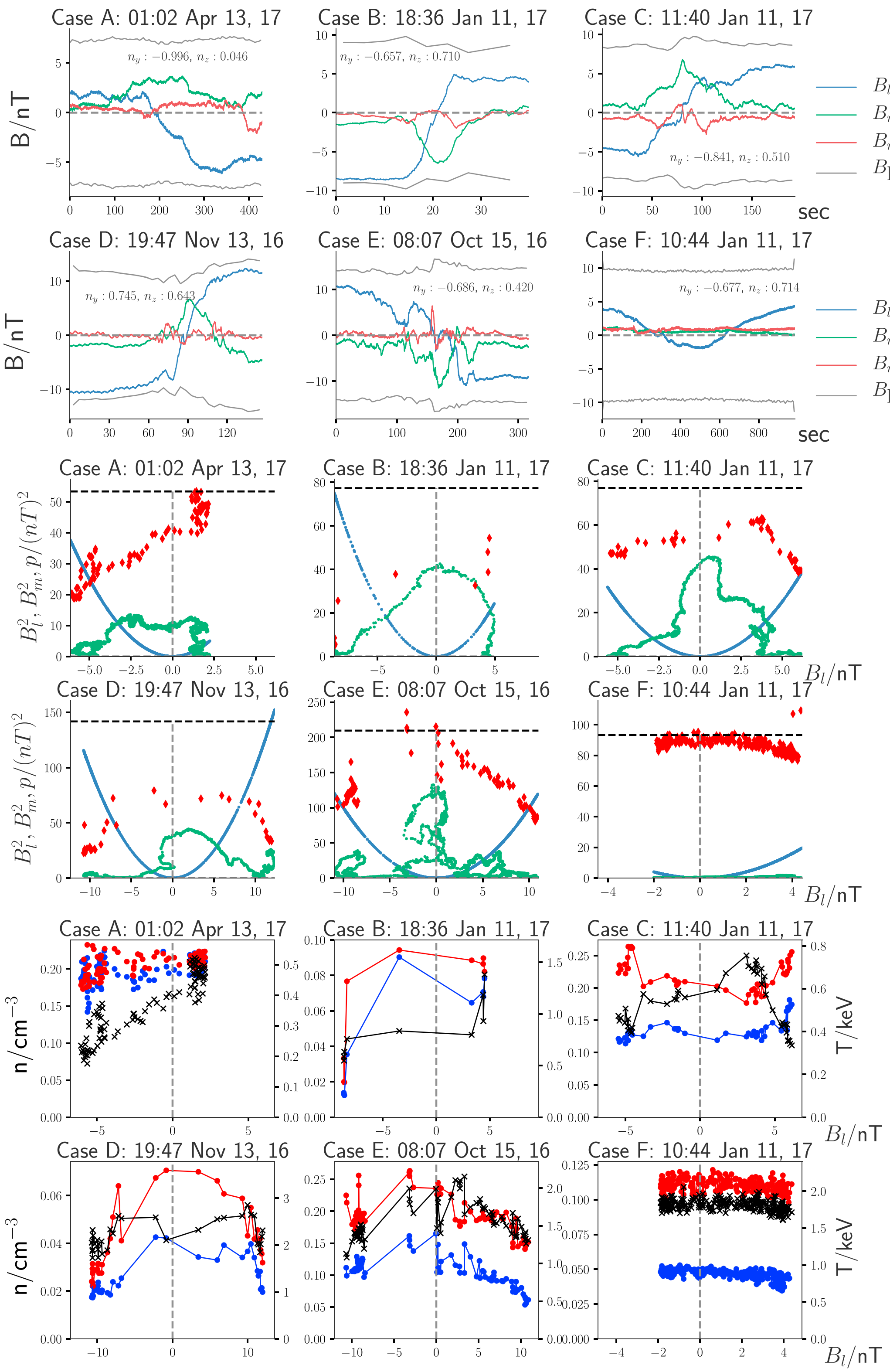

Figure 2. The top six panels show time series of magnetic field components and the lobe magnetic field (grey curve). The middle six panels show the pressure components B_l^2(blue), B_m^2(green), and $p = 2\mu_0 k_B n_e (T_i + T_e)$ (red), and the top dashed lines indicate the average lobe pressure. The bottom six panels show distributions of the density (black cross), ion (red), and electron (blue) temperatures across the sheet. The electron temperature is multiplied by 5.

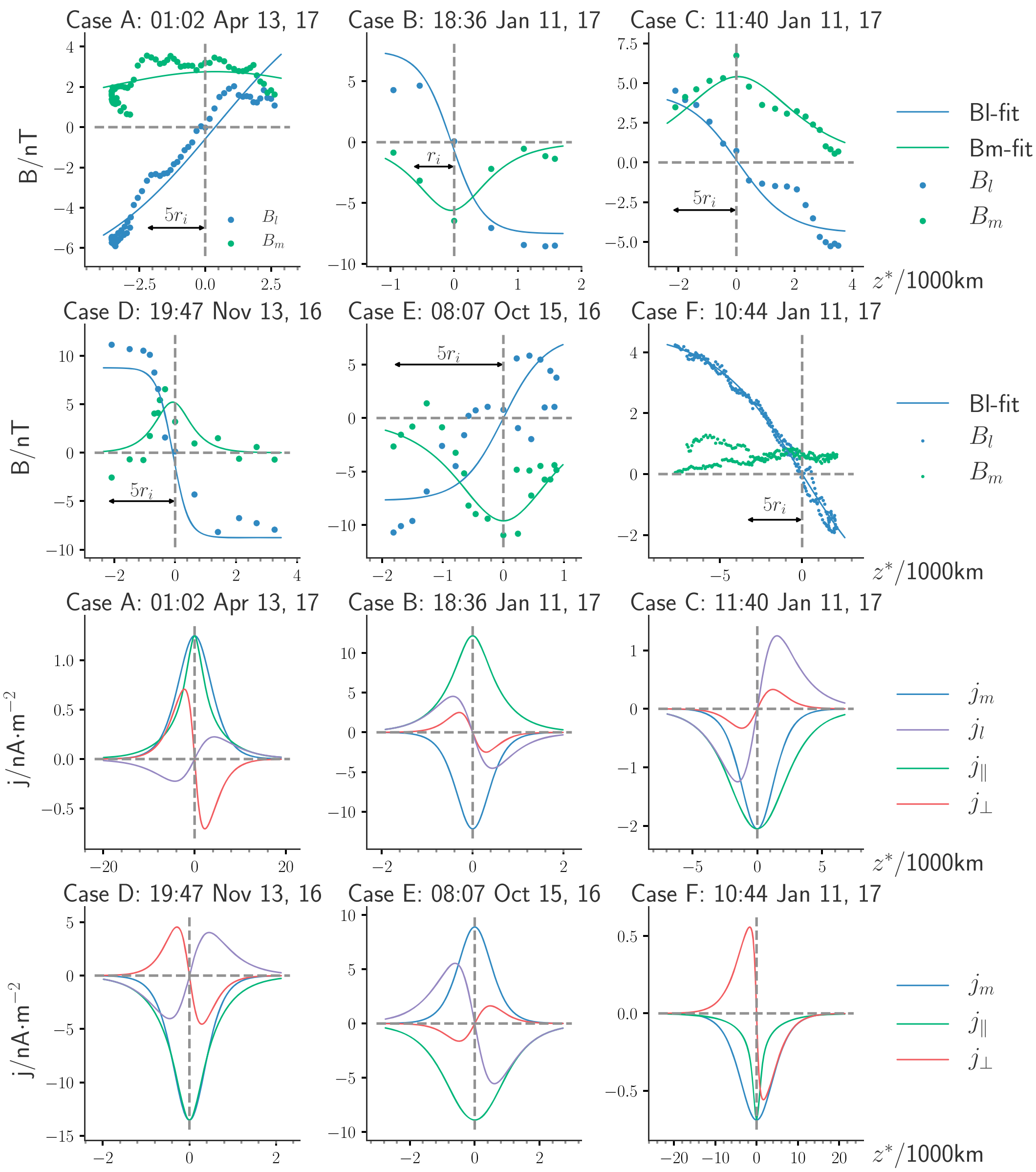

Figure 3. The top six panels show the reconstructed spatial profile of B_l, B_m; the bottom six panels show $j_l, j_m, j_\parallel$, and $j_\perp$ profiles.

near-Earth magnetotail reconnection region is located between the well-investigated near-Earth current sheet (distances $\sim$ 15–20 R_E) with strong transverse cross-tail currents (see statistics of Cluster results in Petrukovich et al., 2015; Runov et al., 2006) and the lunar distance current sheet ($\sim$50–60 R_E) with intense cross-tail field-aligned currents. The stability of these two types of current sheets may be a factor that controls the location and regime of near-Earth reconnection. Therefore, further investigation (e.g., with Magnetospheric Multiscale mission; Burch et al., 2016) of current sheets located in intermediate distances (distances $\sim$ 25–50 R_E) is required to understand magnetotail reconnection physics.

In about 50% of magnetotail current sheet crossings by the ARTEMIS probes at lunar distances, an usually strong B_m peak around the equatorial plane $B_l = 0$ was observed. During these events, the current sheets were tilted, with the normal directed partially along dawn-dusk. In these current sheets the B_m (which results from both B_z and B_y GSM components) contributes more than 30% of the pressure balance. Such current sheets are expected to appear when the plasma pressure is insufficient to balance the lobe pressure $\sim B^2_{\text{lobe}}$. Although unusual in the near-Earth magnetotail, they have been found in the rarefied plasma of Jupiter's magnetotail (Artemyev et al., 2014) and in the cold plasma of Venus' and Mars' magnetotails (Artemyev et al., 2017; Rong et al., 2015). In Jupiter's magnetotail, the current sheet geometry is determined by a strong planetary magnetic field, and observed field-aligned currents are part of the global magnetosphere current system. Mars' and Venus' magnetotails are formed mainly by the solar wind magnetic field, and current sheets in these magnetotails resemble solar wind rotational discontinuities (e.g., Paschmann et al., 2013, and references therein). Current sheets in the Earth's lunar distance magnetotail represent an intermediate state between these two systems: depending on geomagnetic conditions and magnetotail dynamics, they can be situated on the magnetic field connected to Earth and populated by hot rarefied plasma from the near-Earth magnetotail (like current sheets in Jupiter's magnetotail) or they can be connected to IMF lines and be populated by cold magnetosheath plasma (like current sheets in Mars' and Venus' magnetotails). Whether these field-aligned currents are closed through the ionosphere (like field-aligned currents generated in the near-Earth magnetotail) or are a part of the locally closed magnetotail current system is unknown and needs to be investigated with global models.

Acknowledgments
We acknowledge NASA contract NAS502099 for the use of data from the THEMIS Mission and NSF/GEM grant 1503097 for financial support. We thank C. W. Carlson and J. P. McFadden for the use of ESA data; D. E. Larson and R. P. Lin for the use of SST data; and K. H. Glassmeier, U. Auster, and W. Baumjohann for the use of FGM data provided under the lead of the Technical University of Braunschweig and with financial support through the German Ministry for Economy and Technology and the German Aerospace Center (DLR) under contract 50 OC 0302. The THEMIS data were downloaded from http://themis.ssl.berkeley.edu/.

References

Angelopoulos, V., Sibeck, D., Carlson, C. W., McFadden, J. P., Larson, D., Lin, R. P., et al. (2008). First results from the THEMIS mission. *Space Science Reviews*, *141*, 453–476. https://doi.org/10.1007/s11214-008-9378-4

Artemyev, A. V., Angelopoulos, V., Halekas, J. S., Runov, A., Zelenyi, L. M., & McFadden, J. P. (2017). Mars's magnetotail: Nature's current sheet laboratory. *Journal of Geophysical Research: Space Physics*, *122*, 5404–5417. https://doi.org/10.1002/2017JA024078

Artemyev, A. V., Vasko, I. Y., & Kasahara, S. (2014). Thin current sheets in the Jovian magnetotail. *Planatary Space Science*, *96*, 133–145. https://doi.org/10.1016/j.pss.2014.03.012

Auster, H. U., Glassmeier, K. H., Magnes, W., Aydogar, O., Baumjohann, W., Constantinescu, D., et al. (2008). The THEMIS fluxgate magnetometer. *Space Science Reviews*, *141*, 235–264. https://doi.org/10.1007/s11214-008-9365-9

Birn, J., Schindler, K., & Hesse, M. (2004). Thin electron current sheets and their relation to auroral potentials. *Journal of Geophysical Research*, *109*, A02217. https://doi.org/10.1029/2003JA010303

Burch, J. L., Moore, T. E., Torbert, R. B., & Giles, B. L. (2016). Magnetospheric multiscale overview and science objectives. *Space Science Reviews*, *199*, 5–21. https://doi.org/10.1007/s11214-015-0164-9

Eastwood, J. P., Hietala, H., Toth, G., Phan, T. D., & Fujimoto, M. (2015). What controls the structure and dynamics of Earth's magnetosphere? *Space Science Reviews*, *188*, 251–286. https://doi.org/10.1007/s11214-014-0050-x

Fan, F., Huang, C., Lu, Q., Xie, J., & Wang, S. (2016). The structures of magnetic islands formed during collisionless magnetic reconnections in a force-free current sheet. *Physics of Plasmas*, *23*(11), 112106. https://doi.org/10.1063/1.4967286

Harrison, M. G., & Neukirch, T. (2009). One-dimensional Vlasov-Maxwell equilibrium for the force-free Harris sheet. *Physical Review Letters*, *102*(13), 135003. https://doi.org/10.1103/PhysRevLett.102.135003

Hoshino, M., Nishida, A., Mukai, T., Saito, Y., Yamamoto, T., & Kokubun, S. (1996). Structure of plasma sheet in magnetotail: Double-peaked electric current sheet. *Journal of Geophysical Research*, *101*, 24,775–24,786. https://doi.org/10.1029/96JA02313

McFadden, J. P., Carlson, C. W., Larson, D., Ludlam, M., Abiad, R., Elliott, B., et al. (2008). The THEMIS ESA plasma instrument and in-flight calibration. *Space Science Reviews*, *141*, 277–302. https://doi.org/10.1007/s11214-008-9440-2

Nakamura, R., Baumjohann, W., Fujimoto, M., Asano, Y., Runov, A., Owen, C. J., et al. (2008). Cluster observations of an ion-scale current sheet in the magnetotail under the presence of a guide field. *Journal of Geophysical Research*, *113*, A07S16. https://doi.org/10.1029/2007JA012760

Paschmann, G., Haaland, S., Sonnerup, B., & Knetter, T. (2013). Discontinuities and Alfvenic fluctuations in the solar wind. *Annales Geophysicae*, *31*, 871–887. https://doi.org/10.5194/angeo-31-871-2013

Petrukovich, A. A., Artemyev, A. V., Vasko, I. Y., Nakamura, R., & Zelenyi, L. M. (2015). Current sheets in the Earth magnetotail: Plasma and magnetic field structure with Cluster project observations. *Space Science Reviews*, *188*, 311–337. https://doi.org/10.1007/s11214-014-0126-7

Pulkkinen, T. I., Baker, D. N., Owen, C. J., Gosling, J. T., & Murphy, N. (1993). Thin current sheets in the deep geomagnetic tail. *Geophysical Research Letters*, *20*, 2427–2430. https://doi.org/10.1029/93GL01590

Rong, Z. J., Barabash, S., Stenberg, G., Futaana, Y., Zhang, T. L., Wan, W. X., et al. (2015). The flapping motion of the Venusian magnetotail: Venus Express observations. *Journal of Geophysical Research: Space Physics*, *120*, 5593–5602. https://doi.org/10.1002/2015JA021317

Rong, Z. J., Wan, W. X., Shen, C., Li, X., Dunlop, M. W., Petrukovich, A. A., et al. (2012). Profile of strong magnetic field B_y component in magnetotail current sheets. *Journal of Geophysical Research*, *117*, A06216. https://doi.org/10.1029/2011JA017402

Runov, A., Sergeev, V. A., Nakamura, R., Baumjohann, W., Apatenkov, S., Asano, Y., et al. (2006). Local structure of the magnetotail current sheet: 2001 Cluster observations. *Annales Geophysicae*, *24*, 247–262.

Sergeev, V., Angelopoulos, V., Carlson, C., & Sutcliffe, P. (1998). Current sheet measurements within a flapping plasma sheet. *Journal of Geophysical Research*, *103*, 9177–9188. https://doi.org/10.1029/97JA02093

Sibeck, D. G., & Lin, R.-Q. (2014). Size and shape of the distant magnetotail. *Journal of Geophysical Research: Space Physics*, *119*, 1028–1043. https://doi.org/10.1002/2013JA019471

Sitnov, M. I., & Merkin, V. G. (2016). Generalized magnetotail equilibria: Effects of the dipole field, thin current sheets, and magnetic flux accumulation. *Journal of Geophysical Research: Space Physics*, *121*, 7664–7683. https://doi.org/10.1002/2016JA023001

Sonnerup, B. U. Ö., & Cahill Jr., L. J. (1968). Explorer 12 observations of the magnetopause current layer. *Journal of Geophysical Research*, *73*, 1757. https://doi.org/10.1029/JA073i005p01757

Vasko, I. Y., Petrukovich, A. A., Artemyev, A. V., Nakamura, R., & Zelenyi, L. M. (2015). Earth's distant magnetotail current sheet near and beyond lunar orbit. *Journal of Geophysical Research: Space Physics*, *120*, 8663–8680. https://doi.org/10.1002/2015JA021633

Wilson, F., Neukirch, T., Hesse, M., Harrison, M. G., & Stark, C. R. (2016). Particle-in-cell simulations of collisionless magnetic reconnection with a non-uniform guide field. *Physics of Plasmas*, *23*(3), 032302. https://doi.org/10.1063/1.4942939

Zelenyi, L. M., Malova, H. V., Artemyev, A. V., Popov, V. Y., & Petrukovich, A. A. (2011). Thin current sheets in collisionless plasma: Equilibrium structure, plasma instabilities, and particle acceleration. *Plasma Physics Reports*, *37*, 118–160. https://doi.org/10.1134/S1063780X1102005X

Zhang, T. L., Baumjohann, W., Nakamura, R., Balogh, A., & Glassmeier, K. (2002). A wavy twisted neutral sheet observed by CLUSTER. *Geophysical Research Letters*, *29*(19), 1899. https://doi.org/10.1029/2002GL015544

Zhou, F., Huang, C., Lu, Q., Xie, J., & Wang, S. (2015). The evolution of the ion diffusion region during collisionless magnetic reconnection in a force-free current sheet. *Physics of Plasmas*, *22*(9), 092110. https://doi.org/10.1063/1.4930217